Observations of Unsteady Separated-Type Cavitation in Convergent-Divergent Channel

Keiichi SATO* **Hirokazu NAKAMURA***
Yasuhiro SAITO*

Abstract Unsteady collapsing behavior in the separated shear-layer cavitation is known to be highly impulsive, so it is investigated using a convergent-divergent channel. In addition, the cavity behaviors are investigated in detail in the separated vortex flow using a high-speed video camera triggered by impact pressure accompanied with the cavity collapse. As a result, it is reported that the impulsive force at cavitation collapse can be related to the shedding of cloud-like cavitation in the transition-cavitation stage and the periodic shedding motion can be considered as a self-exciting phenomenon with a reentrant motion. The coalescence of vortex cavitation bubbles on the separated shear layer and the reentrant motion of unsteady fixed-type cavity cause the periodic shedding motion of cloud-like cavitation.

Key words : Cavitation, Cavitation Impact, High Speed Video System, Self-Exciting Motion

1. INTRODUCTION

Cavitation generates high impact energy and, as a result, brings about some critical problems such as the performance reduction, noise and erosion in fluid machinery. On the other hand, from a positive viewpoint, cavitation bubbles can also make an applicable role on the concentration of fluid energy.

According to some investigations (e.g. Sato & Sugimoto 1997, Sato et al. 2000), the occurrence of high impulsive pressure with the collapse of cavitation bubbles depends on the type and the developing stage of cavitation. Especially, a vortex-type cavitation is focused on, which is periodically shed downstream from a fixed-type cavity (Knapp, 1955). Many studies about this type of cavitation have been made, especially, from a viewpoint of hydrofoil cavitation in relation to a ship propeller and an impeller of turbomachinery (Avellan et al. 1988, Le et al. 1993, de Lange et al. 1994, Kawanami et al. 1997, Pham et al. 1999, Kjeldsen et al. 2000).

Recently, it is, through the cavitation study of a long cylindrical orifice, indicated by the authors (Sato & Saito, 2001) that the periodic behavior of cloud-like cavities can be considered as a self-exciting phenomenon with the feedback mechanism and the vortex formation. In addition, a cavitating flow in a convergent-divergent channel attracts large attention because of the expected existence of the similar mechanism with a shedding-type cloud cavitation on the hydrofoil. A typical research (Selim & Hutton 1981) on the convergent-divergent channel cavitation made clear that this kind of cavitation can produce severe erosion, especially in the direction of the rotational axis of vortex cavitation. Hutton (1986) also showed that the unsteady motion of fixed-type cavity was related to the motion of a reentrant jet and the shedding of cloud-like

* Kanazawa Institute of Technology, 7-1 Ogigaoka, Nonoichi-Machi, Ishikawa, 921-8501
TEL (076)248-9214 FAX(076)294-6704 E-mail:ksato@neptune.kanazawa-it.ac.jp

cavitation. Callenaere, Franc & Michel (1998) showed the existence zone of periodical cavitation through some experiments about the effects of the throat height and divergent angle in the convergent-divergent channel.

In the present study, the separated-vortex-type cavitation is examined using a high-speed-video camera to make clear the detailed appearance of vortex cavitation bubbles including the collapsing motion of cloud-like cavitation. It is found that the high impulsive region can be related to the transition stage of cavitation and the regular shedding motion of cloud-like cavitation is produced by the coalescence of vortex cavitation bubbles on the separated shear layer and the reentrant motion of unsteady cavity.

2. Experimental

The experiment was conducted using a small cavitation tunnel of a closed re-circulating type shown in **Fig.1** (Sato, 1994). Two channels were used as the test section with different throat heights of H=40mm (channel A) and 30mm (channel B) as shown in **Figs. 2** and **3**. **Fig.2** shows the test section (channel A) to observe a side-view of a convergent-divergent channel. **Fig.3** shows the test section (channel B) to observe the span-view. The blockage ratio is 0.5 for both the channels A and B. In all cases the upstream velocity of the test section was kept constant at U=3.47 m/s.

The measurement system is shown in **Fig.4**. The details of bubble motion were taken with a high-speed video camera (Kodak, Extapro Model 4540, Maximum frame speed = 40500 fps) triggered by an impulsive signal from an accelerometer (TEAC, 0.3-50 KHz ± 3dB) fixed on the outer wall of the test section. This high-speed video system can take a high-speed picture of bubble behaviors before and behind a trigger point (Sato & Ogawa, 1995). The position of the accelerometer is shown as "Y" in the distance of X downstream of the throat in the convergent-divergent channel as shown in **Figs. 2 or 3**. The sidewall of the test section on which an accelerometer was fixed was made of acrylic resin for channel A, and stainless steel for channel B. The cavitation condition in the present experiment was adjusted by lowering the tunnel static pressure under constant velocity condition.

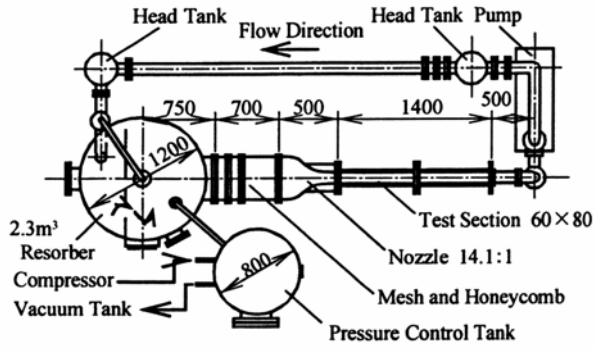

Fig.1 Cavitation tunnel

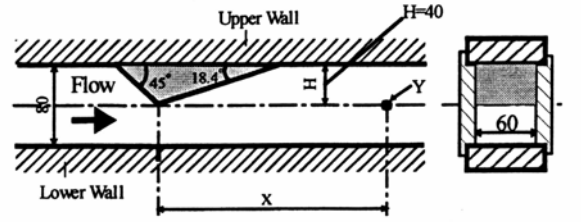

Fig.2 Contraction and divergence channel for side-view observation (channel A)

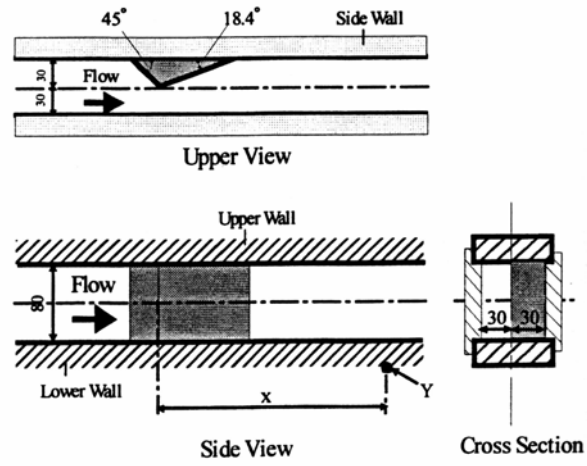

Fig.3 Contraction and divergence channel for span-view observation (channel B)

The cavitation number σ, Reynolds number Re and Strouhal number St are defined as follows,

$$\sigma = 2(P_\infty - P_V)/\rho U^2 \quad \cdots\cdots (1)$$

$$Re_c = U_c \cdot H/\nu \quad \cdots\cdots (2)$$

$$St = fH/U_c. \quad \cdots\cdots (3)$$

Here, P_v, P_∞, U and U_c are saturated vapor pressure,

static pressure and uniform velocity of upstream condition, and U_c, H are average throat velocity and throat height of convergent-divergent channel, respectively. In addition, ν, T_w and β are kinetic viscosity, water temperature and dissolved gas content of water, respectively, and F_s is video frame rate of high-speed video camera. Strouhal number St is based on the throat height H.

3. EXPERIMENTAL RESULTS AND DISCUSSIONS

3.1 Cavitation Developing Process and Its Impact Characteristics

With decreasing cavitation number, the cavitation state changes from the non-cavitation stage to the incipient cavitation, sub-cavitation, transition-cavitation and supercavitation stage. These stages can be closely connected with the extent of cavitation noise and erosion (Sato & Sugimoto 1997, Hutton & Fry 1983), as well as the appearance of cavitation.

In order to examine the cavitation state in the present experiment (Test section A), the cavitation impulsive acceleration was detected with an accelerometer fixed on the outer sidewall of the test section. Some typical results are shown in **Fig.5**. The results were obtained at the measurement position of x=400 mm (x/H=10).

With decreasing cavitation number, the acceleration rises around σ =13 to reach the incipient cavitation stage, where the rms-value of impulsive acceleration at non-cavitation stage is chosen as a reference one. Thus, the stage becomes the sub-cavitation one, where the acceleration characteristics keep almost constant or have a weak decreasing tendency after the mild peak as shown in **Fig.5**. Next, the stage changes to the transition cavitation, where a sharp impact peak is produced. It is considered that this stage with a sharp peak has high impulsive pulses and, as the result, high erosion. With further decreasing cavitation number, the stage changes to the supercavitation when the acceleration level drops rapidly.

It should be noticed that the acceleration level in **Fig.5** is very high because the measurement position of x/H=10 is approximately in the center of large erosive

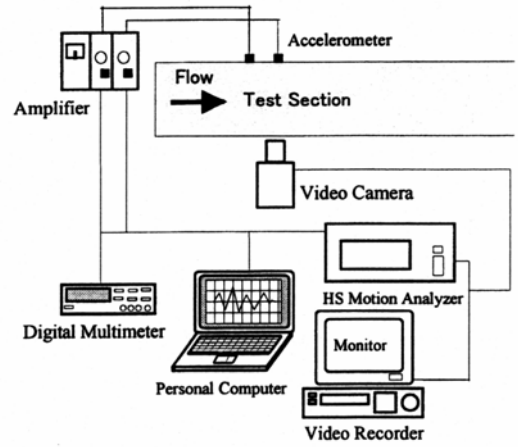

Fig.4 Measurement and observation system

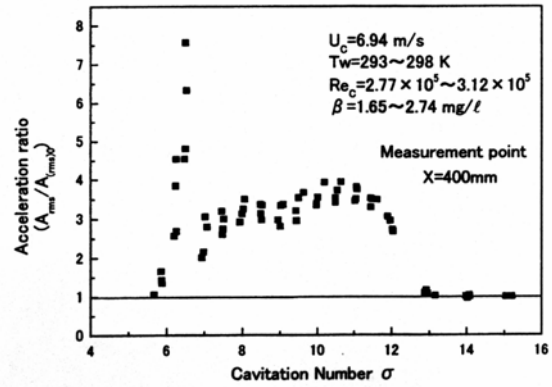

Fig.5 Variation of impulsive acceleration ratio with cavitation number (channel A: side-view)

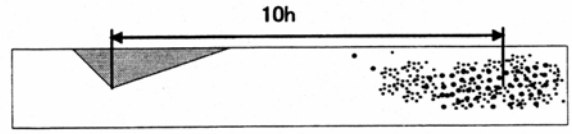

σ =6.5
Re_c=2.75×10^5~3.18×10^5
U_c=6.94 m/s
Tw=292.8~299 K
β =1.61~2.52 mg/ℓ

Fig.6 Sketch of erosion pit distribution

region. This fact was also confirmed by a cavitation erosion test. In the present research, the erosion test was conducted using the sidewall made from an aluminum plate in the same test section as shown in **Fig.2**. The cavitation number was set to be σ =6.5. **Fig.6** shows an erosion pit distribution on the aluminum plate. As the result, the erosion pits were caused in the area with the center around the position of x=10H downstream of the throat in the convergent-divergent channel, so that it was confirmed

that this installation point of the accelerometer was appropriate to the measurement of cavitation impact.

A series of variations in the impulsive acceleration, on the other hand, is in agreement with the time-averaged appearance of cavitation shown in **Fig.7**. For cavitation numbers of σ =10 to 12 near the incipient cavitation stage, cavitation bubbles cannot be clearly taken because of the low number density of bubbles, while the cavitation impulse itself shows a relatively large value. The reason may be that there is little interference between each bubble at this stage. Next, with decreasing cavitation number the number density of bubbles increases so that the cavitating-zone length appears to increase step by step. It should be noted, however, that there is some empty room without a sufficient number of bubbles inside the separated region behind the throat. It occurs just near the wall surface of the divergent nozzle. In the case of **Fig.7**, the

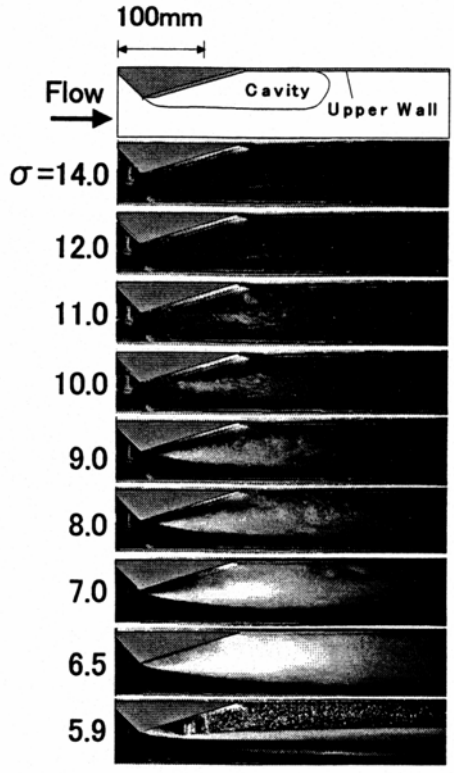

Fig.7 Change of time-averaged cavitating zone (channel A: side-view)

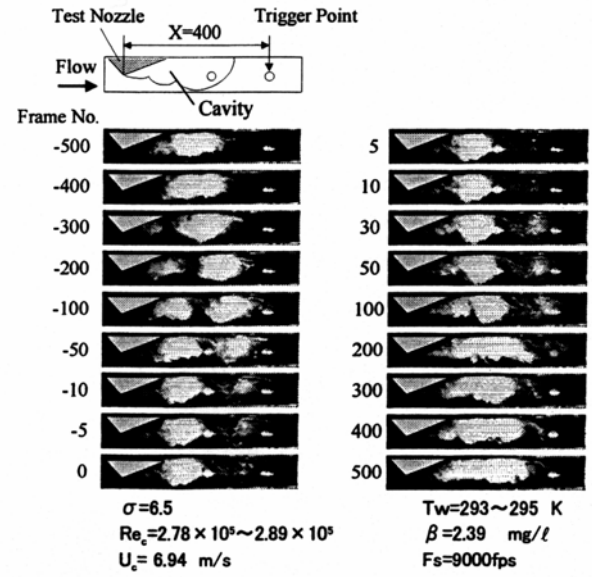

Fig.8 Shedding behavior of cloud-like cavity in a convergent-divergent nozzle

separation region is almost completely covered white by cavitation bubbles when the cavitation number reaches the value of σ =6.5. The stage of this cavitation number corresponds to the transition-cavitation region where very high impulsive acceleration can be measured as shown in **Fig.5**. After this stage, the cavitating region rapidly increases in length and changes to a clear long cavity, namely the supercavitation stage.

3.2 Shedding Process of Vortex Cavitation in Transition-Cavitation Stage

(1) Whole appearance of cavitation and reentrant motion just behind the throat

It is possible to relate the high cavitation impact near the transition-cavitation region at σ =6.5 with the bubble aspect. This can be conducted by taking a high-speed photography of the bubble aspect. **Fig.8** shows high-speed video images of the bubble appearance in the transition-cavitation stage. It is found that the aspect is much different from the above-mentioned time-averaged aspect because the cavitation bubbles are formed as a cluster type and shed downstream. The cloud-like cavity is shed with clear periodicity to the downstream direction and thereafter it collapses to emit large impact pressure. In **Fig.8**, the shedding cavity collapses near Frame No. 0 and emits large impact pressure. The rebound motion is shown

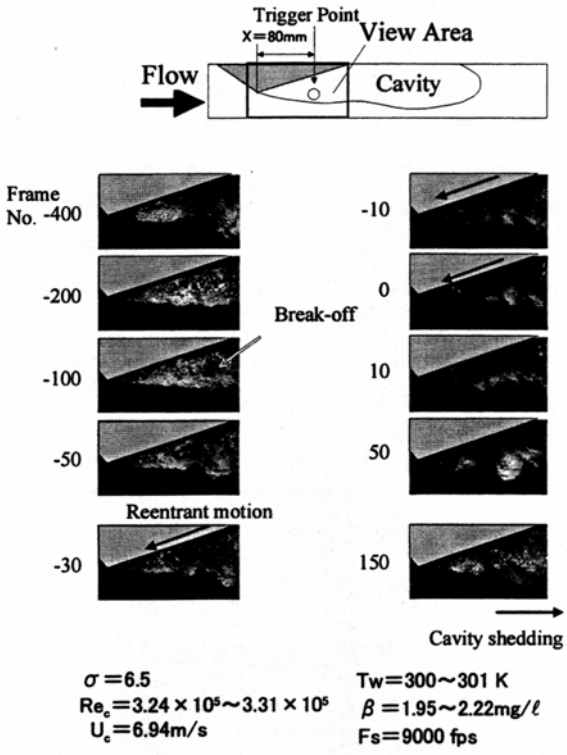

Fig.9 Detailed behavior of cavity near the throat of channel

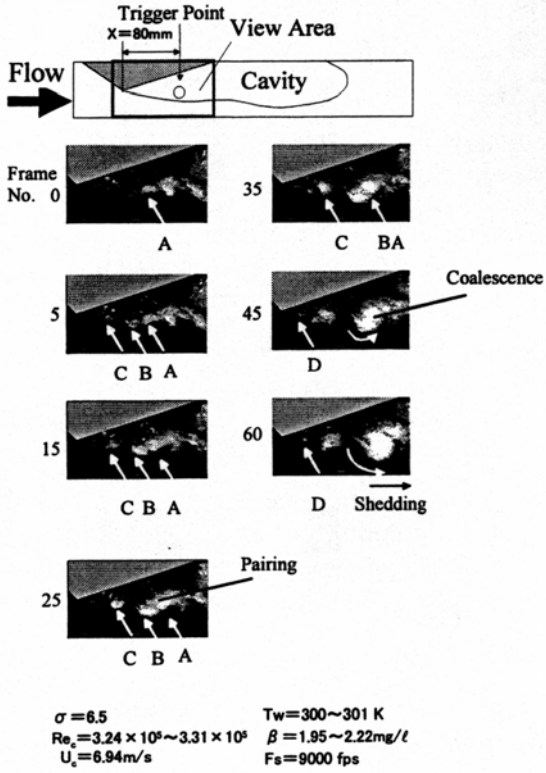

Fig.10 Behavior of micro-vortex cavities on the separated shear layer

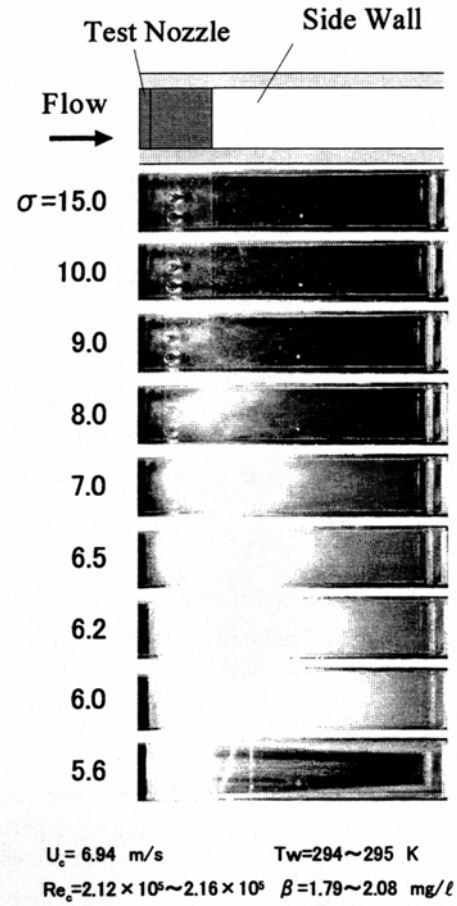

Fig.11 Change of time-averaged cavitating zone (channel B: span-view)

around Frame No. 30-100 and then a cluster of cavitation bubbles disappears again.

The formation and shedding process of the cavitation cluster in the transition-cavitation region is interesting, and may be important as the cavitation impact mechanism connected with cavitation noise and erosion. Since the behavior of separated vortex cavitation just behind the throat is little clearly shown in **Fig.8**, the details are shown in **Fig.9** where the pictures were taken in 9000 fps (frames/s). As shown by Frame No.-400 to -100 in **Fig.9**, the separated vortex cavitation grows as a vortex cavity, while it is greatly involved just behind the throat. Thereafter, the vortex cavity breaks off around Frame No.-100 to -50 and a part of it is shed to the downstream direction. The cavitation cluster left upstream disappears partially as the result of forming the counter flow motion (reentrant motion) along the wall surface of the divergent division

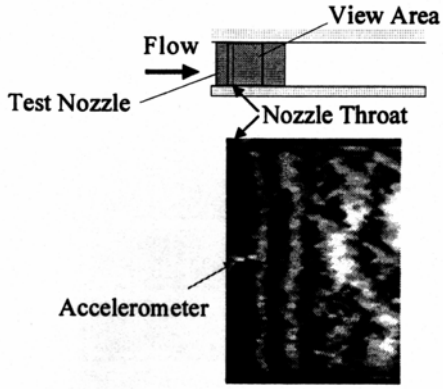

σ=6.3 Tw=297～299 K
Re_c=2.27×10⁵～2.38×10⁵ β=1.89～2.24 mg/ℓ
U_c= 6.94 m/s Fs=9000fps

Fig.12 Appearance of transverse vortex cavities just behind nozzle throat

as shown in Frame No.-50 to 0. The reentrant motion appears to have reached just the throat top around Frame No.0. The behavior of micro-vortices on the separated shear layer is visualized by cavitating the vortices in Frame No.0-150 in **Fig.9**.

The details in small vortex cavities are shown in **Fig.10**. It is found that the small vortex cavities are formed on the separated shear layer (Frame No. 5 in **Fig.10**: cavities A, B, C). These vortex cavities move to the downstream direction. The cavities A and B show a pairing and coalescing motion each other (Frame No.15-45). An existence of a new vortex cavity (cavity D) can be clearly confirmed around the picture No.45. Around Frame No.60 in **Fig.10**, the coalescing cavity (A and B) is shed downstream, the cavity C grows to a larger scale and begins to form a new attached cavity together with the new cavity D. Thus, new separation vortex cavities grow through the formation and coalescence of such vortices, and finally change to a shedding cavity as well as a new attached cavity.

(2) Span-wise aspect of shedding-type vortex cavitation

The span-wise observation of cavitation aspect was made in the convergent-divergent nozzle (channel B) as shown in **Fig.3**. The time-averaged aspect of cavitation in this case is shown in **Fig.11**. The cavitation bubbles just after the throat is shown in **Fig.12** to examine the details of bubble occurrence using a high-speed video camera. It is found that the cavitation after the throat appears to be almost two-dimensional at the first stage and then transits to the complex three-dimensional aspect at the downstream position through the development and coalescence of cavities as mentioned in the next part.

In this test channel (channel B), a large impact peak is shown at about σ=6.2-6.3. High-speed video images of the cavitation aspect in the transition cavitation region (σ=6.3) are shown in **Fig.13**. The cavitation bubble is shed periodically as a cloud-like

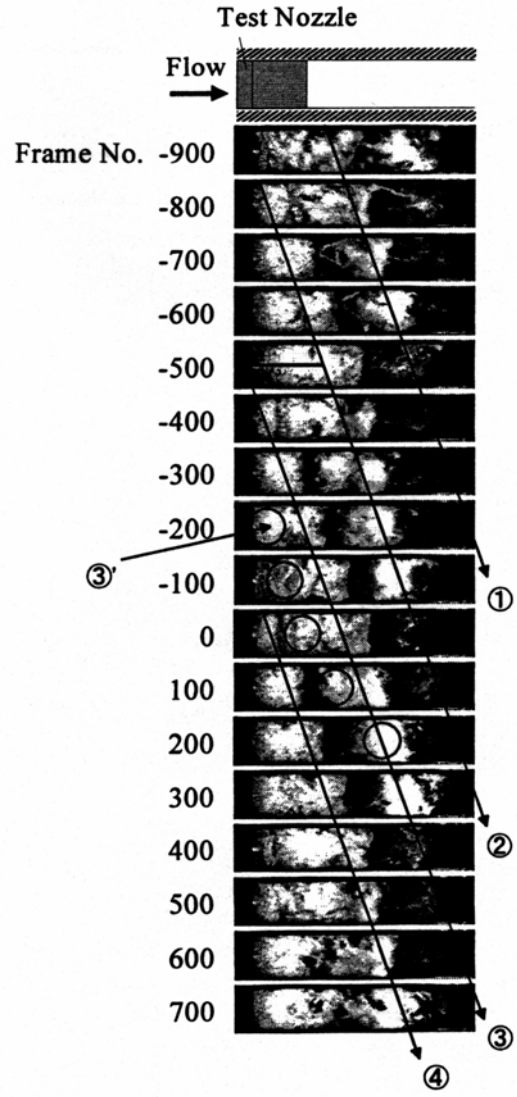

σ=6.3 Tw=297～299 K
Re_c=2.25×10⁵～2.37×10⁵ β=1.96～2.30 mg/ℓ
U_c= 6.94 m/s Fs=9000 fps

Fig.13 Periodic shedding behavior of cloud-like cavity and the coalescence process (span-view)

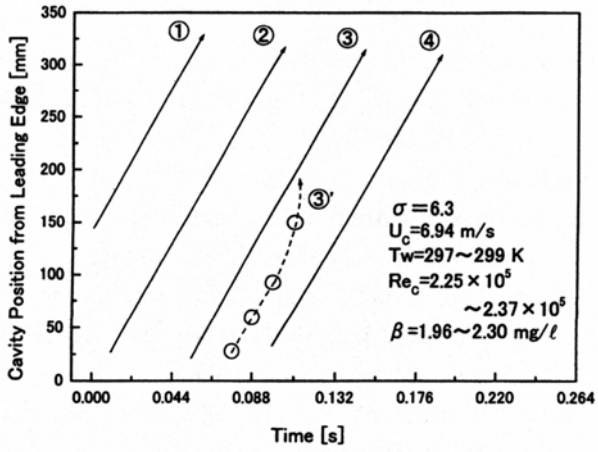

Fig.14 Loci of shedding cavities

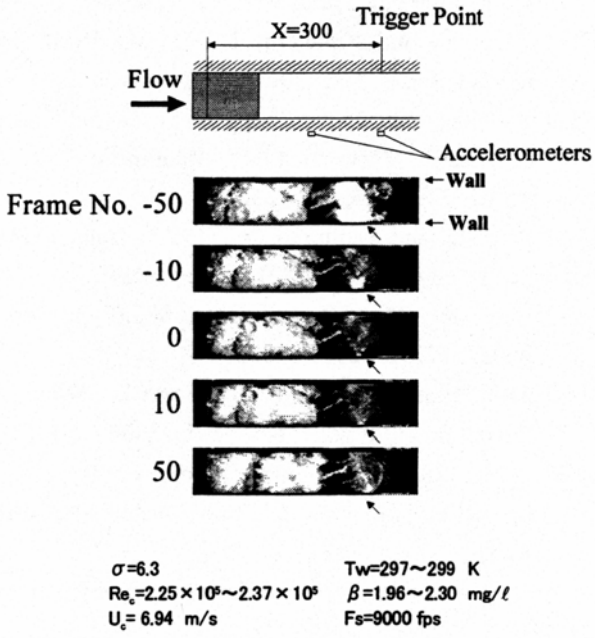

Fig.15 Collapsing motion of shedding cloud-like cavity (Impinge toward side-wall)

cavity to the downstream direction, as easily readable from the pictures. Within the scope of **Fig.13** there are four cycles of cavity shedding process, where four lines ①, ②, ③ and ④ are approximately drawn across the picture to show the shedding process. From the pictures it is found that there are the clear periodic shedding of cloud-like cavities and the coalescence of vortex cavities at the stage of cavity growth (e.g. Frame No.-400 to 200, for line ③ and ③' in **Fig.13**). Near the throat of the convergent-divergent nozzle, several vortex cavities are formed as shown in **Fig.10** or Frame No.-200 to 0 in **Fig.13**. These vortex cavities coalesce with the main cavity and shed downstream as shown in the line ①~③.

Fig.14 shows the loci of shedding cavities estimated from **Fig.13**. The dotted line shows an approximate locus of the sub-cavity that coalesces with the main shedding cavity on the way. This coalescence can correspond to that in **Fig.10** (cavities A and B). It is found the shedding is almost periodic in frequency and constant in speed. The shedding Strouhal number St of the cloud-like cavitation to the downstream direction is estimated to be about 0.095 on average.

At about Frame No.-100 (or No.-900, 400) in **Fig. 13**, the bubble cluster of cavitation near the throat disappears, and this fact is correspondent to the aspect in which the reentrant motion arrives near the throat area that is flow separation point, as shown in Frame No. 0 of **Fig.9** mentioned before. At that time, vortex cavitation bubbles on the separated shear layer occur and grow through the coalescence of small vortices as shown in **Figs. 10** and **13**. From an enlarged view of the aspect near the throat as shown in **Figs. 9** and **12**, it can be found that vortex cavitation is formed from several thin transverse vortices. It grows as one vortex cavity through the coalescence of the small vortices and the existing large cavity to shed downstream. Shedding cavitation bubble collapses downstream so that it emits large impact pressure and sometimes causes cavitation damage on the wall surface.

Fig.15 shows the aspect in which the shedding bubble cluster collapses to the direction of the wall surface. It collapses in the arrow point of Frame No.0. The accelerometer was installed on the external wall, and Frame No. 0 was at the detection point of impact acceleration. The bubble behavior was taken before and behind the detection signal used as a trigger for high-speed video camera system. It is found that a large cluster of cavitation bubbles violently collapses toward the channel sidewall and causes a rebound motion afterwards once the bubble collapses and shrinks.

4. CONCLUDING REMARKS

For the purpose of the elucidation on the mechanism of high impact cavitation, the separated vortex cavitation was experimentally examined by a high-speed video observation, etc. A convergent

-divergent nozzle was chosen as a cavitation flow channel, which showed a representative type of separated vortex cavitation. The main results are obtained as follows.

1. The unsteady cloud-like cavity closely related to the highly impulsive cavitation first arises from a micro-vortex cavity on the separated shear layer near the channel throat (separation point), and then grows to the large scale through some coalescences of small vortex cavities. It causes the reentrant motion as well as the periodic shedding motion after it grows to a certain scale.

2. The cloud-like cavitation related with the formation, coalescence and growth of vortex cavities, is periodically shed downstream through the feedback motion of the reentrant jet formed along the bottom of fixed cavity toward the leading separation point.

3. The periodic shedding cavity rapidly collapses in the downstream area and, as a result, forms the high impact.

4. Large impact peak is formed at the transition-cavitation stage on the way to the supercavitation stage from the sub-cavitation one. This impact peak has close relation to the unsteady cloud-like cavities formed by separated vortex cavitation.

5. ACKNOLEDGMENTS

The authors are grateful to Messrs. A. Oomori, A. Takenaka and Y. Tanaka in Kanazawa Institute of Technology for their assistance in the experiments. This work is supported by the Grant-in-Aid for the Scientific Research of the Ministry of Education, Science and Culture of Japan.

REFERENCES

[1] Avellan, F., Dupont, P. and Ryhming, I., (1988) Proc. 17th ONR Symp. on Naval Hydrodynamics, 317-329.

[2] Callenaere, M., Franc, J.-P. and Michel, J. M., (1998) Proc. Third Int. Symp. on Cavitation, Grenoble, 209-214.

[3] Hutton, S.P. and Fry, S.A., (1983) Proc. IMechE, Cavitation, C222, 269-276.

[4] Hutton, S. P., (1986) Proc. Int. Symp. on Cavitation, Sendai, 21-29.

[5] Kawanami, Y., Kato, H., Yamaguchi, H., Tanimura, M. and Tagaya, Y., (1997) Trans. ASME, J. Fluids Eng., 119, 788-794.

[6] Knapp, R.T., (1955) Trans. ASME, 77, 1045-1054.

[7] Kjeldsen, M., Arndt, R.E.A. and Effertz, M., (2000) Trans. ASME, J. Fluids Eng., 122, 481-487.

[8] de Lange, D. F., de Bruin, G. J. and van Wijngaarden, L., (1994) Proc. The Second Int. Symp. on Cavitation, Tokyo, 45-49.

[9] Le, Q., Franc, J.P. and Michel, J.M., (1993) Trans. ASME, J. Fluids Eng., 115, 243-248.

[10] Pham, T.M., Larrarte, F. and Fruman, D.H., (1999) Trans. ASME, J. Fluids Eng., 121, 289-296.

[11] Sato, K. and Kakutani, K., (1994) JSME Int. Journal, Ser. B, 37-2, 306-312.

[12] Sato, K. and Ogawa, N., (1995) Cavitation and Gas-Liquid Flow in Fluid Machinery Devices, ASME, FED-226, 119-125.

[13] Sato, K. and Sugimoto, Y., (1997) Trans. JSME, Ser. B, 63-616, 3815-3821, (in Japanese).

[14] Sato, K., Saito, Y. and Ohta, H., (2000) Proc. ASME, FEDSM2000-11023, 1-7.

[15] Sato, K. and Saito, Y., (2001) Forth Int. Symp. on Cavitation - CAV2001, Pasadena, A9-003, 1-8.

[16] Selim, S. M. A. and Hutton, S. P., (1981) Cavitation Erosion in Fluid Systems, ASME, 15-25.